ISSN 0915-633X

NATIONAL INSTITUTE FOR FUSION SCIENCE

Electromagnetic Microinstabilities in Helical Systems

H. Sugama and T.-H. Watanabe

(Received - Jan. 23, 2004)

NIFS-793 Feb. 2004

TOKI, JAPAN

Electromagnetic microinstabilities in helical systems

H. Sugama and T.-H. Watanabe

National Institute for Fusion Science, Graduate University for Advanced Studies

Toki 509-5292, Japan

(Dated: January 22, 2004)

Electromagnetic microinstabilities in helical systems are studied by numerically solving integral eigenmode equations, which are derived from the ion gyrokinetic equation, the quasineutrality equation, the Ampère's law, and the massless electron approximation. The stellarator expansion technique is used to evaluate finite-beta effects on the guiding-center drift in the helical configuration, where the toroidal plasma shift and the magnetic shear strongly influence the magnetic curvature and accordingly the stability of both magnetohydrodynamics (MHD) and kinetic modes. The kinetic integral equations are shown to reduce to the ideal MHD ballooning mode equation in the fluid limit, from which the Mercier criterion is obtained. For helical geometry like the Large Helical Device (LHD), it is confirmed that, when increasing the beta value, the ion temperature gradient (ITG) mode is stabilized while the kinetic ballooning mode (KBM) is destabilized due to the unfavorable geodesic curvature resulting from the negative magnetic shear combined with the toroidal plasma shift. Also, dependencies of these kinetic-mode properties on the poloidal wave number and the magnetic shear are investigated. It is found that the KBM-unstable parameter region is narrower than the Mercier-unstable region in the LHD-like configuration.

Keywords: kinetic ballooning mode, ITG mode, gyrokinetics, helical system

PACS numbers: 52.35.Py, 52.35.Qz, 52.55.Hc

I. INTRODUCTION

Microinstabilities in magnetically confined plasmas have been studied extensively as a key mechanism for producing plasma turbulence and resultant anomalous transport [1]. Above all, ion temperature gradient (ITG) modes and turbulence driven by them are most actively investigated by numerous theories and simulations in recent years [2]. The ITG mode is essentially an electrostatic instability, which is more unstable for lower-beta plasmas, and electromagnetic microinstabilities such as the kinetic ballooning mode (KBM) [3] are anticipated to become an active source of turbulence and transport in high-beta regimes. For the ITG mode, electrons are often assumed to adiabatically respond to electrostatic fluctuations while, in the electromagnetic case, it is necessary to include more complicated nonadiabatic electron dynamics due to magnetic fluctuations. So far, for helical systems, theoretical studies of microinstabilities have also been concerned with electrostatic modes mainly [4–6] and those of electromagnetic modes have not been done sufficiently compared with tokamak cases. Since, recently, helical systems such as the Large Helical Device (LHD) [7] have succeeded in producing high-beta plasmas, understanding the physical mechanism of their anomalous transport requires electromagnetic-microinstability analyses. Also, electromagnetic microinstabilities are deeply related to the ideal magnetohydrodynamics (MHD) interchange and ballooning modes with short wave lengths. In the LHD, a large pressure gradient is observed even in the Mercier-unstable region [7, 8]. Therefore, it is interesting to examine how the stability criterion based on the ideal MHD is modified by the microinstability analysis, which takes account of kinetic effects such as the Landau damping and the finite gyroradii.

In the present work, we investigate electromagnetic microinstabilities in helical systems with the LHD-like magnetic configuration. Recently, the kinetic ballooning mode in the LHD was also studied by Yamagishi *et al.* [9] using the ordinary differential eigenmode equation derived by Tang *et al.* [3], in which the poloidal wave length is assumed to be much larger than the

ion thermal gyroradius. Here, in order to fully take account of the finite-gyroradius effect on the electromagnetic mode, we use the kinetic integral eigenmode equations similar to those by Dong *et al.* for tokamaks [10], which are derived from the ion gyrokinetic equation [11, 12], the quasineutrality condition, the Ampère's law, and the massless electron approximation. Our numerical solution to the kinetic integral eigenmode equations utilizes procedures by Sugama [13] for proper analytic continuation of the dispersion relation in the complex frequency plane, by which we can calculate both positive and negative growth rates so as to accurately determine the critical condition for the marginal stability.

Helical ripples and safety-factor profiles in the LHD-like configuration present a striking contrast to those in tokamaks. The ideal MHD ballooning mode in tokamaks is stable for the negative magnetic shear $dq/dr < 0$ (q: the safety factor, r: the minor radius) while, as shown by Nakajima [14], the unfavorable geodesic curvature resulting from the negative shear combined with a toroidal (Shafranov) shift of the finite-beta helical plasma destabilizes the ballooning mode in the LHD configuration. Here, we employ the stellarator expansion method [15] to evaluate the finite-beta toroidal shift, which critically affects local magnetic shear, magnetic curvature, guiding-center drift, and resultantly stability of both MHD and kinetic modes. The kinetic eigenmode equations are shown to reduce to the ideal MHD ballooning equation in the fluid limit, from which the Mercier criterion for the helical plasma is obtained. Then, we can make a comparison between kinetic results from the microinstability analysis and the Mercier criterion.

The rest of this paper is organized as follows. In Sec. II, equilibria of helical plasmas are treated by the stellarator expansion technique to derive useful formulas for evaluation of the toroidal plasma shift and the magnetic drift for the finite-beta case. The kinetic integral eigenmode equations for electromagnetic microinstabilities are derived in Sec. III. A and the ideal MHD ballooning equation is obtained from them in the fluid limit in Sec. III. B, where we also derive the Mercier criterion which takes account of the finite-beta helical configuration by using the formulas in Sec. II. In Sec. IV, the kinetic integral eigenmode equations are numerically solved to investigate dependencies of electromagnetic-mode properties on the plasma beta, the magnetic shear, and the poloidal wave number. There, the relation of the kinetic results to the Mercier parameter is also examined. Finally, conclusions are given in Sec. V.

II. EQUILIBRIA OF HELICAL PLASMAS

Here, we use the toroidal coordinates (r, θ, ζ), where r, θ, and ζ denote the minor radius, the poloidal angle, and the toroidal angle, respectively, and they are related to the conventional cylindrical coordinates (R, ϕ, Z) with

$$R = R_0 + \Delta(r) + r\cos\theta, \quad \phi = -\zeta, \quad Z = r\sin\theta. \tag{1}$$

Here the point defined by $R = R_0$ and $Z = 0$ represents the geometrical center of the poloidal cross section of the wall boundary (or the external helical coils), and $\Delta(r)$ is defined later.

In the stellarator expansion [15], the lowest-order poloidal flux function $\psi \equiv -(4\pi^2 R_0)^{-1} \int \mathbf{B}\cdot\nabla\theta dV$ is independent of ζ, and is written as $\psi = A + \psi_h$. Here A is the toroidal (ζ) component of the magnetic vector potential associated with the plasma current and ψ_h represents the contribution from the external helical fields. The function A is determined by

$$\nabla_\perp^2 A = -4\pi\Omega\frac{dp}{d\psi} + G(\psi), \tag{2}$$

where $\nabla_\perp^2$ denotes the two-dimensional Laplacian in the plane perpendicular to the toroidal direction, the equilibrium pressure $p(\psi)$ and $G(\psi)$ are flux functions and Ω is given by

$$\Omega = \frac{2(R - R_0)}{R_0} + \Omega_h. \tag{3}$$

Here, Ω_h is associated with the contribution of the helical field to the averaged magnetic curvature. Hereafter, we assume that there is no net toroidal current and that $\psi_h = \psi_h(r_0)$ and

$\Omega_h = \Omega_h(r_0)$ are functions of $r_0 \equiv [(R-R_0)^2+Z^2]^{1/2} \simeq r + \Delta(r)\cos\theta$ only, where r_0 is the minor radius measured from the center (or magnetic axis) of the vacuum helical field. Now, we take $\psi = \psi(r)$ so that the poloidal cross section labeled by ψ is a circle with the radius r, the center of which is shifted from $R = R_0$ by $\Delta(r)$ ($\ll r$). Neglecting small terms $\sim (\Delta/r)^2$, Eq. (2) is rewritten as

$$\nabla_\perp^2 [\psi(r) - \psi_h(r) - \Delta(r)\psi_h'(r)\cos\theta] \simeq -4\pi \frac{p'(r)}{\psi'(r)} \left[\frac{2r}{R_0}\cos\theta + \Omega_h(r)\right] + G(r), \tag{4}$$

where $' \equiv d/dr$ and the pressure gradient p' is regarded as a small quantity of $O(\Delta/r)$. We obtain $G(r) = 4\pi\Omega_h(r)p'(r)/\psi'(r)$ from the no net toroidal current condition, $\langle \nabla_\perp^2 A\rangle = 0$, where $\langle\cdot\rangle$ denotes the flux surface average. Then, separating Eq. (4) into the θ-averaged part and the θ-dependent part, we find $\psi(r) = \psi_h(r)$ and

$$(\Delta\psi')'' + \frac{(\Delta\psi')'}{r} - \frac{\Delta\psi'}{r^2} = 4\pi \frac{p'}{\psi'}\frac{2r}{R_0}, \tag{5}$$

respectively. Defining the safety factor $q(r) \equiv -rB_0/(R_0\psi'(r))$ and the local plasma beta value $\beta(r) \equiv 8\pi p(r)/B_0^2$, and using Eq. (5) yield

$$\Delta(r) = R_0 q(r) \int_0^r \frac{dx}{x^3} \int_0^x y^2 q(y)\beta'(y)dy + \frac{q(r)\Delta(0)}{q(0)}, \tag{6}$$

where the toroidal shift $\Delta(0)$ of the magnetic axis can experimentally be controlled by the external vertical field. [Equation (6) is equivalent to Eq. (7.112) in Freidberg [16].] From Eq. (6), we can show

$$\Delta'(r) = \frac{R_0 q(r)}{r^3} \int_0^r x^2 q(x)\beta'(x)dx + \hat{s}(r)\frac{\Delta(r)}{r}, \tag{7}$$

and

$$r\Delta''(r) = -\alpha(r) + [2\hat{s}(r) - 3]\Delta'(r) + [2\hat{s}(r) - \hat{s}^2(r) + r\hat{s}'(r)]\frac{\Delta(r)}{r}, \tag{8}$$

where the magnetic shear parameter $\hat{s}(r) \equiv rq'(r)/q(r)$ and $\alpha(r) \equiv -R_0 q^2(r)\beta'(r)$ are defined. The toroidal force balance for the finite-beta case causes the toroidal axis shift and the poloidal field compression, which are taken into account by Eqs. (6)–(8). In the well-known s-α model, $|\Delta''| \gg |\Delta'|/r \sim |\Delta|/r^2$ is used and only the first term $-\alpha$ on the right-hand side of Eq. (8) is retained by assuming that the pressure profile has a steep gradient only around the surface considered [see Sec. 10.5.5 in Freidberg [16]]. This term is responsible for the second stabilization of the ballooning mode in high beta regimes. However, it was pointed out by Nakajima [14] following the high beta model by Coppi *et al.* [17] that, in the helical system, the second group of terms $[2\hat{s}(r) - 3]\Delta'(r)$ on the right-hand side should also be kept and combined with the geodesic curvature in order to explain the destabilization mechanism of the ballooning mode for the case of the negative magnetic shear $\hat{s} < 0$. Using the expression for Δ'' in Eq. (8), we can naturally unify the conventional s-α model based on the assumption of the steep pressure gradient and the high beta model by Coppi *et al.* [17] and Nakajima [14] who used the near-axis expansion.

In the ballooning representation [18, 19], we treat the fluctuation which varies rapidly across the field lines and has the wave number vector perpendicular to $\mathbf{b} \equiv \mathbf{B}/B$ denoted by

$$\mathbf{k}_\perp = k_n \frac{\nabla r}{|\nabla r|} + k_t \frac{\mathbf{b}\times\nabla r}{|\nabla r|}. \tag{9}$$

In the present case, the component k_t tangential to the flux surface is approximately equal to the poloidal wave number, $k_t \simeq k_\theta = nq(r)/r$, where n is the toroidal mode number. The ratio Σ of the normal component k_n to the tangential one k_t is written as

$$\Sigma \equiv \frac{k_n}{k_t} \simeq \hat{s}(\theta - \theta_k) + [\Delta'(1+\hat{s}) + r\Delta'']\sin\theta, \tag{10}$$

where $\mathcal{O}(\Delta')$ terms are neglected except for the term $\Delta'(1+\hat{s})\sin\theta$ that significantly affects the ballooning mode stability. From Eqs. (9) and (10), we have

$$k_\perp^2 = k_\theta^2[1+\Sigma^2]. \tag{11}$$

When evaluating the guiding-center drift which is responsible for ballooning-type instabilities, we take into account effects of helical ripples in the magnetic field strength by using $B = B_0[1-\epsilon_{00}(r)-\epsilon_t(r)\cos\theta-\epsilon_h(r)\cos(L\theta-M\zeta)]$, where L and M are the poloidal and toroidal period numbers of the helical fields, respectively ($L=2$ and $M=10$ for the LHD). Here, $\epsilon_t = r/R_0$ and $\epsilon_h(r)$ ($\propto r^L$) represent the toroidicity and helicity parameters, respectively, and $\epsilon_{00}(r) = \frac{1}{2}[\langle\Omega\rangle+\beta(r)]$ is associated with the averaged normal magnetic curvature and the diamagnetic effect. Then, the magnetic drift frequency for the particle species a with the mass m_a and the charge e_a is given by

$$\omega_D = 2\epsilon_n\omega_{*a}(v_\parallel^2+v_\perp^2/2)v_{Ta}^{-2}G_c(\theta), \tag{12}$$

where $\epsilon_n = L_n/R_0$ is the ratio of the density gradient scale length $L_n \equiv -(d\ln n_0/d\ln r)^{-1}$ to the major radius R_0, $\omega_{*a} \equiv -k_\theta c T_a/(e_a L_n)$ is the diamagnetic frequency, $v_\parallel$ ($v_\perp$) is the parallel (perpendicular) velocity, and $v_{Ta} \equiv (2T_a/m_a)^{1/2}$ is the thermal velocity. Also, the dimensionless curvature factor $G_c(\theta)$ is defined along the field line labeled with $\alpha_0 = \zeta - q\theta$ by

$$\begin{aligned} G_c(\theta) &\equiv R_0[(\mathbf{b}\cdot\nabla)\mathbf{b}\times\mathbf{b}]\cdot(\mathbf{k}_\perp/k_t) \\ &= R_0\langle\Omega\rangle'/2+\cos\theta+L(\epsilon_h/\epsilon_t)\cos\{(L-Mq)\theta-M\alpha_0\} \\ &\quad +\Sigma(\theta)[\sin\theta+L(\epsilon_h/\epsilon_t)\sin\{(L-Mq)\theta-M\alpha_0\}]. \end{aligned} \tag{13}$$

Unfavorable (favorable) curvature is indicated by $G_c > 0$ (< 0). On the right-hand side of Eq. (13), the first term is derived from the averaged normal curvature, the second and third terms correspond to the normal curvature due to the toroidicity and the helicity while the fourth and fifth terms with the coefficient Σ contain effects of the toroidal and helical geodesic curvature, respectively. From Eqs. (1) and (3), the averaged normal curvature term $\langle\Omega\rangle'$ is written as

$$\langle\Omega\rangle' = \Omega_h'(r) + \frac{2}{R_0}\langle\Delta+r\cos\theta\rangle'. \tag{14}$$

Here, from Ref. 20, the averaged helical curvature is expressed in terms of q and $\hat{s}$ as

$$\Omega_h'(r) = \frac{M}{L}\frac{(r^4/q)'}{R_0^2r^2} = \frac{M}{L}\frac{r}{R_0^2q}(4-\hat{s}). \tag{15}$$

The contribution of the toroidal plasma shift to the normal curvature is represented by

$$\frac{2}{R_0}\langle\Delta+r\cos\theta\rangle' = \frac{[(r^2\Delta)'/r]'}{R_0} = \frac{1}{R_0}\left[-\alpha(r)+2\hat{s}\Delta'+(2\hat{s}-\hat{s}^2+r\hat{s}')\frac{\Delta}{r}\right], \tag{16}$$

where Eqs. (6)–(8) and $\langle\cdot\rangle \simeq \oint\cdot(1+\Delta'\cos\theta)d\theta/(2\pi)$ are used. We see from Eqs. (8), (10), (13), (14), and (16) that $\alpha > 0$ included in Δ'' reduces G_c and accordingly contributes to stabilization by entering both the averaged normal curvature term $\langle\Omega\rangle'$ and the Σ term combined with the geodesic curvature. In helical systems with negative magnetic shear $\hat{s} < 0$, destabilization occurs from an increase in G_c due to $\hat{s}\Delta' > 0$ that also appears in both $\langle\Omega\rangle'$ and Σ.

In the next section, the gyrokinetic analysis of electromagnetic microinstabilities in helical plasmas is carried out based on the geometrical expressions shown in this section.

III. EIGENMODE EQUATIONS

A. EIGENMODE EQUATIONS

The distribution function in the $(\mathbf{x},\mathbf{v})$ phase space for the species $a = i$ (ion) or e (electron) is divided into the equilibrium and perturbation parts as $f_a = n_0F_{Ma} + \delta f_a$ where n_0 is the

equilibrium density and $F_{Ma} \equiv \pi^{-3/2} v_{Ta}^{-3} \exp(-v^2/v_{Ta}^2)$ is the Maxwellian distribution function. In the magnetic field $\mathbf{B}$, the perturbation part δf_a with the perpendicular wave number vector $\mathbf{k}_\perp$ is written as

$$\delta f_a = -\frac{e_a \phi}{T_a} n_0 F_{Ma} + h_a e^{-i\mathbf{k}_\perp \cdot \boldsymbol{\rho}_a}, \tag{17}$$

where ϕ represents the electrostatic potential, $\boldsymbol{\rho}_a \equiv \mathbf{b} \times \mathbf{v}/\Omega_a$ denotes the gyroradius vector, and $\Omega_a \equiv e_a B/(m_a c)$ is the gyrofrequency. Here, the first and second terms on the right-hand side of Eq. (17) represent the adiabatic and nonadiabatic parts, respectively. The nonadiabatic distribution function h_a is independent of the gyrophase and is described in the collisionless linear electromagnetic case by the gyrokinetic equation [11, 12],

$$\left[\frac{v_\parallel}{R_0 q}\frac{\partial}{\partial \theta} - i(\omega - \omega_{Da})\right] h_a = -i\left(\omega - \omega_{*Ta}\right) n_0 F_{Ma} J_0(k_\perp \rho_a) \frac{e_a}{T_a}\left(\phi - \frac{v_\parallel}{c} A_\parallel\right), \tag{18}$$

where $A_\parallel = \delta \mathbf{A} \cdot \mathbf{b}$ is the parallel component of the vector potential for the magnetic field perturbation, ω_{Da} is given by Eq. (12) and

$$\omega_{*Ta} = \omega_{*a}\left[1 + \eta_a\left\{\left(\frac{v}{v_{Ta}}\right)^2 - \frac{3}{2}\right\}\right]. \tag{19}$$

Here, J_0 is the Bessel function of order zero and $\eta_a \equiv d \ln T_a / d \ln n_0$ is the ratio of the temperature gradient to the density gradient. In Eq. (18), we have neglected the parallel magnetic field perturbation and used the ballooning representation to regard the poloidal angle θ as a coordinate along the magnetic field line which forms the so-called *covering space* $(-\infty < \theta < +\infty)$ [18, 19].

Throughout this work, following Dong *et al.* [10], effects of magnetic geometry in helical systems are considered only through the magnetic drift and the perpendicular wave number vector described in the previous section. Trapped particle effects and variation in the parallel velocity $v_\parallel$ along the field line are neglected because such instabilities as the ITG mode and the ballooning mode treated here are driven by passing particles mainly. Then, the solution of Eq. (18) with the boundary conditions $\lim_{\theta \to \pm\infty} h_a(\theta) = 0$ is given by

$$h_a = \begin{cases} -i \int_{-\infty}^{\theta} d\theta' (R_0 q/|v_\parallel|) e^{i\zeta_a(\theta,\theta')} (\omega - \omega_{*Ta}) \\ \quad \times n_0 F_{Ma} J_0(k'_\perp \rho_a) \frac{e_a}{T_a}\left(\phi - \frac{v_\parallel}{c} A_\parallel\right) \quad \text{for } v_\parallel > 0 \\ -i \int_{\theta}^{+\infty} d\theta' (R_0 q/|v_\parallel|) e^{-i\zeta_a(\theta,\theta')} (\omega - \omega_{*Ta}) \\ \quad \times n_0 F_{Ma} J_0(k'_\perp \rho_a) \frac{e_a}{T_a}\left(\phi - \frac{v_\parallel}{c} A_\parallel\right) \quad \text{for } v_\parallel < 0, \end{cases} \tag{20}$$

where $k'_\perp$ is given by Eq. (32) and

$$\zeta_a(\theta, \theta') = \int_{\theta'}^{\theta} d\theta'' (R_0 q/|v_\parallel|)[\omega - \omega_{Da}(\theta'')]. \tag{21}$$

In the ballooning representation, the boundary conditions $\lim_{\theta \to \pm\infty} \phi(\theta) = \lim_{\theta \to \pm\infty} A_\parallel(\theta) = 0$ are also employed. Using the solution given by Eq. (20), we can calculate the density perturbation, $\delta n_a \equiv \int d^3v\ \delta f_a = -n_0 e_a \phi / T_a + \int d^3v J_0(k_\perp \rho_a) h_a$, and the parallel current perturbation, $\delta J_\parallel \equiv \sum_{a=i,e} e_a \int d^3v\ J_0(k_\perp \rho_a) h_a v_\parallel$.

In the same way as in Dong *et al.* [10], we here take the limit of the small electron-ion mass ratio, $m_e/m_i \to +0$. Then, we see that, in Eq. (18) for electrons ($a = e$), the terms proportional to the parallel velocity ($v_\parallel \sim v_{Te}$) are dominant and their balance yields the constraint for the lowest order of $A_\parallel$ in the $(m_e/m_i)^{1/2}$-expansion,

$$\int_{-\infty}^{+\infty} dk\ A_\parallel(k) = 0, \tag{22}$$

where $k \equiv |\hat{s} k_\theta|(\theta - \theta_k)$ is used as an independent variable instead of θ. Equation (22) implies that the electric field integrated along the field line $\int E_\parallel dl = i(\omega/c) \int A_\parallel dl$ should vanish in order to

forbid unlimited acceleration of massless electrons. The quasineutrality condition $\sum_{a=i,e} e_a \delta n_a = 0$ is rewritten as

$$
\begin{aligned}
&(1+\tau_e)\phi(k) \\
&= \int_{-\infty}^{+\infty} \frac{dk'}{\sqrt{2\pi}} \left[K_{11}^i(k,k')\phi(k') + \left\{ K_{12}^i(k,k') + K_{12}^e(k,k') \right\} \frac{v_{Ti}}{c} A_\parallel(k') \right],
\end{aligned} \tag{23}
$$

where $\tau_e \equiv T_e/T_i$. From the Ampère's law $k_\perp^2 A_\parallel = 4\pi \delta J_\parallel / c$, we obtain

$$
\begin{aligned}
&\frac{\partial}{\partial k}\left(\frac{1}{2\tau_e} k_\perp^2 \frac{v_{Ti}}{c} A_\parallel(k) \right) \\
&= \frac{\partial}{\partial k}\left(\int_{-\infty}^{+\infty} \frac{dk'}{\sqrt{2\pi}} \left[\left\{ K_{21}^i(k,k') + K_{21}^e(k,k') \right\} \phi(k') + \left\{ K_{22}^i(k,k') + K_{22}^e(k,k') \right\} \frac{v_{Ti}}{c} A_\parallel(k') \right] \right).
\end{aligned} \tag{24}
$$

When using the Ampère's law to determine the lowest order of $A_\parallel$ in the $(m_e/m_i)^{1/2}$-expansion, there simultaneously appear terms including an unknown low-order part of $A_\parallel$ which are not negligible. However, these terms are independent of k so that, in Eq. (24), they are eliminated by taking differential with respect to k.

In Eqs.(23) and (24), the integral kernels due to ions are defined by

$$
\begin{aligned}
\begin{bmatrix} K_{11}^i(k,k') & K_{12}^i(k,k') \\ K_{21}^i(k,k') & K_{22}^i(k,k') \end{bmatrix} &= -i \int_0^{+\infty} \omega_{*e} d\tau \frac{\sqrt{2} e^{i\omega\tau}}{\sqrt{a\lambda}(1+a)} e^{-(k-k')^2/4\lambda} \Gamma_0(k_\perp, k'_\perp) \\
&\times \left[\frac{\omega}{\omega_{*e}} \tau_e + 1 - \frac{3}{2}\eta_i + \frac{\eta_i (k-k')^2}{4a\lambda} \right. \\
&\left. + \frac{2\eta_i}{(1+a)} \left(1 - \frac{k_\perp^2 + k_\perp'^2}{2(1+a)\tau_e} + \frac{k_\perp k'_\perp}{(1+a)\tau_e} \frac{I_1}{I_0} \right) \right] \\
&\times \begin{bmatrix} 1 & -\frac{(k-k')}{2\sqrt{a\lambda}} \\ \frac{\beta_i}{\tau_e} \frac{(k-k')}{2\sqrt{a\lambda}} & -\frac{\beta_i}{\tau_e} \frac{(k-k')^2}{4a\lambda} \end{bmatrix},
\end{aligned} \tag{25}
$$

and those due to electrons are given by

$$
\begin{aligned}
K_{12}^e(k,k') &= i \frac{\sqrt{\pi}}{2\sqrt{2}} \frac{\sqrt{\tau_e} q}{|\hat{s}|\epsilon_n} \left(\frac{\omega}{\omega_{*e}} - 1 \right) \frac{(k-k')}{|k-k'|} \\
K_{21}^e(k,k') &= -\frac{\beta_i}{\tau_e} K_{12}^e(k,k') \\
K_{22}^e(k,k') &= \beta_i \frac{\sqrt{\pi}}{4\sqrt{2}} \left(\frac{q}{\hat{s}\epsilon_n} \right)^2 |k-k'| \\
&\times \left[-\frac{\omega}{\omega_{*e}} \left(\frac{\omega}{\omega_{*e}} - 1 \right) + 2|\hat{s} k_\theta| \epsilon_n \left(\frac{\omega}{\omega_{*e}} - 1 - \eta_e \right) \frac{(k-k')}{|k-k'|} \int_{\theta'}^{\theta} d\theta'' G_c(\theta'') \right].
\end{aligned} \tag{26}
$$

Here, following Dong *et al.* [10], we have used variables defined by

$$
\tau = Rq|\theta - \theta'|/|v_\parallel|, \tag{27}
$$

$$
\lambda = \frac{\tau^2}{\tau_e a} \left(\frac{\hat{s}}{q} \epsilon_n \right)^2 \omega_{*e}^2, \tag{28}
$$

$$
a = 1 + \frac{2i\epsilon_n \omega_{*i} \tau}{(\theta - \theta')} \int_{\theta'}^{\theta} d\theta'' G_c(\theta''), \tag{29}
$$

$$k = |\hat{s}k_\theta|(\theta - \theta_k), \qquad k' = |\hat{s}k_\theta|(\theta' - \theta_k), \tag{30}$$

$$\Gamma_0(k_\perp, k'_\perp) = I_0\left(\frac{k_\perp k'_\perp}{\tau_e(1+a)}\right)\exp\left(-\frac{k_\perp^2 + k_\perp'^2}{2\tau_e(1+a)}\right), \tag{31}$$

$$k_\perp^2 = k_\theta^2[1 + \Sigma^2(\theta)], \qquad k_\perp'^2 = k_\theta^2[1 + \Sigma^2(\theta')]. \tag{32}$$

In Eqs. (23)–(32), the wave numbers k_θ, $k_\perp$, and k are normalized by ρ_s^{-1} with $\rho_s \equiv \sqrt{2T_e/m_i}/\Omega_i$, and I_n is the modified Bessel function of order n. The integral parameter τ in Eqs. (25) and (29) has the opposite sign to that in Dong *et al.* [10] Equations (22)–(24) form coupled integral eigenmode equations which determine the dispersion relation and the mode structure of the electromagnetic instabilities in helical systems. Instead of using the second integral eigenmode equation by Dong *et al.* [see Eq. (13) in Ref. 10], we have employed its derivative with respect to k and the constraint given by Eqs. (24) and (22), respectively, although their eigenmode equations and ours both give the same result for $\theta_k = 0$ because $A_\parallel$ for the most unstable mode is an odd function of k for the unstable mode as shown later. [There seems to be typos in Eqs. (16) and (17) of Dong *et al.*, too.] Also, it is shown in Sec.III.B that, in the fluid limit, the ideal MHD ballooning mode equation is naturally derived from Eqs. (22)–(24), which indicates the validity of our eigenmode equations.

B. IDEAL MHD BALLOONING MODE EQUATION

Here, we consider the fluid limit of Eqs. (22)–(24), in which $|k_\parallel v_{Ti}/\omega| \sim |(v_{Ti}/R_0 q\omega)(\partial/\partial\theta)| \ll 1$, $k_\perp^2\rho_{Ti}^2 \ll 1$, and $|\omega_{Di}/\omega| \ll 1$. It can be shown that, in the fluid limit, the integrals including the ion kernels are approximately written by

$$\int_{-\infty}^{+\infty}\frac{dk'}{\sqrt{2\pi}}K_{11}^i(k,k')\phi(k') \simeq \left[\tau_e + \frac{\omega_{*e}}{\omega} - \left(1 + (1+\eta_i)\frac{\omega_{*e}}{\tau_e\omega}\right)\left(\frac{k_\perp^2}{2} + 2\epsilon_n G_c\frac{\omega_{*e}}{\omega} + \frac{\tau_e v_{Ti}^2}{2R_0^2q^2\omega^2}\frac{d^2}{d\theta^2}\right)\right]\phi, \tag{33}$$

$$\int_{-\infty}^{+\infty}\frac{dk'}{\sqrt{2\pi}}K_{12}^i(k,k')A_\parallel(k') \simeq i\left(1 + (1+\eta_i)\frac{\omega_{*e}}{\tau_e\omega}\right)\frac{\tau_e v_{Ti}}{2R_0q\omega}\frac{dA_\parallel}{d\theta}, \tag{34}$$

$$\int_{-\infty}^{+\infty}\frac{dk'}{\sqrt{2\pi}}K_{21}^i(k,k')\phi(k') \simeq -i\left(1 + (1+\eta_i)\frac{\omega_{*e}}{\tau_e\omega}\right)\frac{\beta_i v_{Ti}}{2R_0q\omega}\frac{d\phi}{d\theta}, \tag{35}$$

$$\int_{-\infty}^{+\infty}\frac{dk'}{\sqrt{2\pi}}K_{22}^i(k,k')A_\parallel(k') \simeq -\left(1 + (1+\eta_i)\frac{\omega_{*e}}{\tau_e\omega}\right)\frac{\beta_i}{2}A_\parallel. \tag{36}$$

Using Eqs. (33)–(36), we can rewrite Eqs. (23) and (24) as ordinary differential equations,

$$\left(1 - \frac{\omega_{*e}}{\omega}\right)\left(\phi - i\frac{R_0q\omega}{2c}\int_{-\infty}^{+\infty}d\theta'\frac{(\theta-\theta')}{|\theta-\theta'|}A_\parallel(\theta')\right) + \left(1 + (1+\eta_i)\frac{\omega_{*e}}{\tau_e\omega}\right)\left[\left(\frac{k_\perp^2}{2} + 2\epsilon_n G_c\frac{\omega_{*e}}{\omega}\right)\phi + \frac{\tau_e v_{Ti}^2}{2R_0q\omega^2}\frac{d}{d\theta}\left(\frac{1}{R_0q}\frac{d\phi}{d\theta} - i\frac{\omega}{c}A_\parallel\right)\right] = 0, \tag{37}$$

and

$$\frac{\partial}{\partial\theta}\left(\frac{1}{2\tau_e}k_\perp^2\frac{v_{Ti}}{c}A_\parallel\right) + i\left(1 + (1+\eta_i)\frac{\omega_{*e}}{\tau_e\omega}\right)\frac{\beta_i v_{Ti}}{2\omega}\frac{d}{d\theta}\left(\frac{1}{R_0q}\frac{d\phi}{d\theta} - i\frac{\omega}{c}A_\parallel\right) + i\frac{\beta_i R_0q\omega}{\tau_e v_{Ti}}\left(1 - \frac{\omega_{*e}}{\omega}\right)\left(\phi - i\frac{R_0q\omega}{2c}\int_{-\infty}^{+\infty}d\theta'\frac{(\theta-\theta')}{|\theta-\theta'|}A_\parallel(\theta')\right) - 2\epsilon_n G_c\frac{\beta_i R_0q\omega_{*e}}{\tau_e v_{Ti}}\left(1 - (1+\eta_e)\frac{\omega_{*e}}{\omega}\right)\frac{R_0q\omega}{2c}\int_{-\infty}^{+\infty}d\theta'\frac{(\theta-\theta')}{|\theta-\theta'|}A_\parallel(\theta') = 0, \tag{38}$$

respectively. Multiplying Eq. (38) with $i\tau_e v_{Ti}/(\beta_i R_0 q\omega)$ and adding it to Eq. (37), we obtain

$$\left(1+(1+\eta_i)\frac{\omega_{*e}}{\tau_e\omega}\right)\left(\frac{k_\perp^2}{2}+2\epsilon_n G_c\frac{\omega_{*e}}{\omega}\right)\phi+i\frac{v_{Ti}}{\beta_i R_0 q\omega}\frac{d}{d\theta}\left(\frac{1}{2\tau_e}k_\perp^2\frac{v_{Ti}}{c}A_\parallel\right)$$
$$-2i\epsilon_n G_c\frac{\omega_{*e}}{\omega}\left(1-(1+\eta_e)\frac{\omega_{*e}}{\omega}\right)\frac{R_0 q\omega}{2c}\int_{-\infty}^{+\infty}d\theta'\frac{(\theta-\theta')}{|\theta-\theta'|}A_\parallel(\theta')=0. \tag{39}$$

For low beta $\beta_i \ll (k_\parallel v_{Ti}/\omega)^2$, we find from Eq. (39) that $|\omega A_\parallel/c| \ll |\partial\phi/\partial\theta|/(R_0 q)$. Then, in this electrostatic case, terms with $A_\parallel$ are neglected in Eq. (37), and we have

$$\frac{\tau_e v_{Ti}^2}{2R_0 q\omega^2}\frac{d}{d\theta}\left(\frac{1}{R_0 q}\frac{d\phi}{d\theta}\right)+\left[\frac{k_\perp^2}{2}+2\epsilon_n G_c\frac{\omega_{*e}}{\omega}+\left(1-\frac{\omega_{*e}}{\omega}\right)\left(1+(1+\eta_i)\frac{\omega_{*e}}{\tau_e\omega}\right)^{-1}\right]\phi=0, \tag{40}$$

which gives the dispersion relation in the fluid limit for electrostatic modes such as the slab and toroidal ITG modes and the electron drift wave.

Next, let us consider the electromagnetic high-beta case. It is found from Eq. (40) that, in the electrostatic fluid limit, $(1-\omega_{*e}/\omega)/(1+(1+\eta_i)\omega_{*e}/(\tau_e\omega))$ is as small as terms of first order in $(k_\parallel v_T/\omega)^2$, $k_\perp^2$, and $|\omega_D/\omega|$. For the electromagnetic case, in which the above electrostatic condition for the eigenfrequency is not satisfied, the lowest-order relation between ϕ and $A_\parallel$ is obtained from Eq. (37) as

$$\phi-\psi_\parallel \equiv \phi - i\frac{R_0 q\omega}{2c}\int_{-\infty}^{+\infty}d\theta'\frac{(\theta-\theta')}{|\theta-\theta'|}A_\parallel(\theta')=0, \tag{41}$$

where $\psi_\parallel \equiv i(R_0 q\omega/2c)\int_{-\infty}^{+\infty}d\theta' A_\parallel(\theta')(\theta-\theta')/|\theta-\theta'|$ is defined [$\psi_\parallel$ should not be confused with the poloidal flux function ψ in Sec. II]. Taking the derivative of Eq. (41) with respect to k yields

$$\frac{1}{R_0 q}\frac{d(\phi-\psi_\parallel)}{d\theta}=\frac{1}{R_0 q}\frac{d\phi}{d\theta}-i\frac{\omega}{c}A_\parallel=0, \tag{42}$$

which represents zero parallel electric field $E_\parallel = 0$ as in the ideal MHD. We also note that, because of the boundary conditions $\lim_{\theta\pm\infty}\phi(\theta)=0$ and $\lim_{\theta\pm\infty}\psi_\parallel(\theta)=0$ derived from Eq. (22), the relation in Eq. (41) is also derived from integrating Eq. (42) without an arbitrary integral constant. Thus, the conditions written in Eqs. (41) and (42) are equivalent to each other. We now use these conditions to eliminate $A_\parallel$ in Eq. (39) and obtain

$$\frac{\partial}{\partial\theta}\left[(1+\Sigma^2)\frac{d\phi}{d\theta}\right]+\left[\frac{R_0^2 q^2}{v_A^2}(1+\Sigma^2)\{\omega^2+(1+\eta_i)(\omega_{*e}/\tau_e)\omega\}+\alpha G_c\right]\phi, \tag{43}$$

where we have defined the Alfvén velocity $v_A \equiv B_0/(4\pi n_0 m_i)^{1/2}$ and used Eq. (11) and the normalized pressure gradient parameter $\alpha \equiv -R_0 q^2 d\beta/dr$ with $\beta \equiv \beta_i+\beta_e \equiv 8\pi n_0(T_i+T_e)/B_0^2$. In Eq. (43), $\omega_{*i}(1+\eta_i) \equiv -(\omega_{*e}/\tau_e)(1+\eta_i)$ represents the diamagnetic frequency associated with the ion pressure gradient. If the magnitude of the eigenmode frequency is much larger than this ion diamagnetic frequency, Eq. (43) reduces to

$$\frac{\partial}{\partial\theta}\left[(1+\Sigma^2)\frac{d\phi}{d\theta}\right]+\left[\frac{R_0^2 q^2}{v_A^2}\omega^2(1+\Sigma^2)+\alpha G_c\right]\phi. \tag{44}$$

which coincides with the ideal MHD ballooning mode equation.

So far, we have confirmed how the ideal MHD ballooning mode equation shown in Eq. (44) is derived from the kinetic integral eigenmode equations in the fluid limit. Then, the interchange stability criterion, namely, the Mercier criterion can be derived from examining the asymptotic behavior of the solution to Eq. (44) for the case of $\omega = 0$ [see Sec. 10.5.4 in Freidberg [16]]. When deriving the Mercier criterion for equilibria of helical plasmas described in the previous section,

we adopt detailed expressions of Σ and G_c given by Eqs. (10) and (13) with help of Eqs. (8), (14), and (16). The resultant Mercier stability criterion is written as

$$D_M \equiv \frac{\alpha}{\hat{s}^2}\left[\frac{R_0}{2}\Omega_h' - \frac{\alpha}{2}\left(1+\frac{L(\epsilon_h/\epsilon_t)}{Mq-L}\right) + \left(\frac{5}{2}\hat{s}-1\right)\Delta' + (2\hat{s}-\hat{s}^2+r\hat{s}')\frac{\Delta}{r}\right] < \frac{1}{4}. \tag{45}$$

In Eq. (45), the term proportional to $L/(Mq-L)(\ll 1)$ may be ignored as a higher-order term in the stellarator expansion. The well-known stabilization due to the magnetic shear is recognized in the denominator of D_M. The normal curvature term $R_0\Omega_h'/2$ associated with the external helical field is a main source of the interchange instability in the helical system. We find that the term proportional to $\alpha \equiv -R_0 q^2 d\beta/dr$ is stabilizing because the Shafranov shift caused by increasing α acts favorably on both normal and geodesic curvatures as seen in the previous section. [It should be noted that the Mercier criterion shown in Eq. (45) contains both normal and geodesic curvature effects.] Also, for typical q profiles in the helical system, we have $2\hat{s}-\hat{s}^2+r\hat{s}' < 0$ and therefore the term proportional to Δ leads to more stability for larger Δ. On the other hand, for negative magnetic shear $\hat{s} \equiv (r/q)(dq/dr) < 0$, the term $(\frac{5}{2}\hat{s}-1)\Delta'$ becomes positive due to the Shafranov shift ($\Delta' < 0$) and thus causes destabilization, which is because $\hat{s}\Delta' > 0$ acts unfavorably on both normal and geodesic curvatures [see Eqs. (8), (10), (13), (14), and (16)]. These qualitative properties described by Eq. (45) agree well with results from more accurate numerical calculations of the Mercier criterion based on the three-dimensional MHD equilibria [21].

IV. NUMERICAL RESULTS

In this section, the coupled integral eigenmode equations shown in Eqs. (22)–(24) are numerically solved to obtain linear growth rates, real frequencies, and mode structures of electromagnetic microinstabilities in a helical system. Employing procedures by Sugama [13] for proper analytic continuation of the dispersion relation in the complex frequency plane, our numerical code can calculate both positive and negative growth rates, which is useful for accurately determining the critical condition for the marginal stability.

Following the study of electrostatic ITG modes by Kuroda *et al.* [4], we consider a system like the LHD and use $L = 2$, $M = 10$, $q = 2$, $\hat{s} = -1$, $\theta_k = 0$, $\alpha_0 = 0$, $\eta_i = \eta_e = 3.5$, $\epsilon_n \equiv L_n/R_0 = 0.3$, $\tau_e \equiv T_e/T_i = 1$, and $\epsilon_h/\epsilon_t = 1$ as standard parameters. Here, $\epsilon_h/\epsilon_t = 1$ corresponds to the magnetic surface $r/a \simeq 0.6$. Also, using $\eta_i = \eta_e = 3.5$ and $\epsilon_n = 0.3$ combined with $R_0 = 3.6\ m$ and $a = 0.6\ m$ gives the density and temperature gradient scale lengths as $L_n = 1.08\ m$ and $L_{Ti} = L_{Te} = 0.36\ m$.

Here, we investigate especially how the plasma beta and the magnetic shear affect linear properties of the microinstabilities through geometrical variation of the helical plasma equilibrium. In the LHD, by applying the vertical field, the vacuum magnetic axis is shifted inward in order to realize good particle confinement. In the presence of the pressure gradient, the Shafranov shift works so as to cancel the inward shift by the vertical field. In the present study, we put $\Delta(r) = 0$ for simplicity, which represents that, because of the counterbalance between the effects of the vertical field and the pressure gradient, the central axis of the magnetic surface considered coincides with that of the external helical coils. We should note that effects of the toroidal plasma shift due to finite beta are still retained through including $\Delta'(r)$ and $\Delta''(r)$. The pressure profile inside the flux surface r is necessary in order to evaluate $\Delta'(r)$ as shown in Eq. (7) although, in numerical calculations here, we follow Coppi *et al.* [17] and Nakajima [14] to use a simple expression

$$\Delta'(r) = -\frac{\alpha(r)}{4}, \tag{46}$$

which is a good approximation to Eq. (7) with $\Delta(r) = 0$ especially for small r. The normalized pressure gradient parameter is rewritten as $\alpha \equiv -R_0 q^2 \beta' = (q^2\beta_i/\epsilon_n)[(1+\eta_i)+\tau_e(1+\eta_e)]$.

The normalized real frequency ω_r/ω_{*e} and growth rate ω_i/ω_{*e} obtained by numerical calculations using the standard parameters described above are plotted as a function of β in Fig. 1.

Figures 1 (a) and (b) correspond to the ITG mode for $k_\theta \rho_{Ti} = 0.5$ and the KBM for $k_\theta \rho_{Ti} = 0.35$, respectively. Here, $k_\theta \rho_{Ti} = 0.5$ and $k_\theta \rho_{Ti} = 0.35$ are the normalized poloidal wave numbers for which the growth rates of the ITG mode and KBM become almost maximum, respectively. Stabilization of the ITG mode and destabilization of the KBM by increasing β are seen in the helical system in the same way as observed in the tokamak case [10] in spite of the opposite sign of the magnetic shear. The eigenfunctions $\phi(\theta)$ and $\psi_\parallel(\theta)$ of the ITG mode for $\beta = 0.008$ and the KBM for $\beta = 0.04$ are shown in Figs. 2 (a) and (b), respectively. We see that the ITG mode is essentially electrostatic ($|\phi| \gg |\psi_\parallel|$) while the KBM approximately satisfies $\phi = \psi_\parallel$ and accordingly the ideal MHD condition $E_\parallel = 0$.

For reference, the averaged normal curvature $R_0\langle\Omega\rangle'/2$ and the Mercier parameter $D_M - 1/4$ are shown as a function of β in Figs. 3 (a) and (b), respectively. Here, we should note that, in Figs. 1 and 3, the magnetic configuration are fixed by the standard parameters. In this case, as β increases, the averaged normal curvature $R_0\langle\Omega\rangle'/2$ monotonically decreases although the Mercier parameter $D_M - 1/4$, which includes effects of both normal and geodesic curvatures as well as the magnetic shear, monotonically increases. It is confirmed in this helical system that the beta value for the marginal stability of the KBM ($\beta \simeq 0.01$) is larger than that for the Mercier marginal stability ($\beta \simeq 0.006$). We also numerically verified that the KBM is completely stabilized for $\beta \geq 0.17$ (not shown in Fig. 1) where the helical system is still Mercier-unstable. Thus, in the present case, the KBM-unstable region is narrower than the Mercier-unstable region. This is a contrast to the tokamak case that is generally Mercier-stable even when the KBM becomes unstable.

Figure 4 shows the normalized real frequency $\omega_r k_\theta \rho_{Ti}/\omega_{*e}$ and growth rate $\omega_i k_\theta \rho_{Ti}/\omega_{*e}$ are plotted as a function of the normalized poloidal wave number $k_\theta \rho_{Ti}$. Here, we employ the $\omega_{*e}/(k_\theta \rho_{Ti})$ as the normalization unit in order to remove the wave number dependence from the unit. Figures 4 (a) and (b) correspond the ITG mode for $\beta = 0$ and the KBM for $\beta = 0.02$, 0.04, and 0.08, respectively. It is seen that the KBM can have much larger growth rates and real frequencies and wider unstable wave number regions than those of the ITG. Therefore, the KMB is considered to be a candidate which causes anomalous transport for high beta values.

Figure 5 (a) shows the normalized real frequency ω_r/ω_{*e} and growth rate ω_i/ω_{*e} of the KBM as a function of the magnetic shear parameter $\hat{s}$ for $k_\theta \rho_{Ti} = 0.35$ and $\beta = 0.01$, 0.02, 0.04, and 0.08. For reference, the averaged normal curvature $R_0\langle\Omega\rangle'/2$ and the Mercier parameter $D_M - 1/4$ are shown as a function of $\hat{s}$ in Figs. 5 (b) and (c), respectively. As seen in Figs. 5 (b) and (c), the stronger negative magnetic shear gives the larger normal curvature but it also leads to the Mercier stability for the low-beta case ($\beta = 0.01$) by the field-line-bending stabilization of the ideal interchange mode. For the high-beta case ($\beta = 0.08$), the Mercier stability is obtained in the weak magnetic shear region ($\hat{s} \gtrsim -0.3$), where both normal and geodesic curvatures become favorable. We find from Fig. 5 (a) that the stronger magnetic shear brings about stabilization of the the electromagnetic microinstability for the lower-beta case, where the mode structure is closer to that of the interchange mode. On the other hand, for higher beta values, the ballooning structure of the kinetic mode becomes more striking and the stronger (negative) magnetic shear enhances destabilization. Thus, low magnetic shear is expected to be favorable for the high-beta plasma confinement. Comparison between Figs. 5 (a) and (c) shows some correlation between the stability of the kinetic mode and the Mercier criterion although we find again that the KBM-unstable region is narrower than the Mercier-unstable region.

V. CONCLUSIONS

In the present paper, collisionless electromagnetic microinstabilities in helical systems are investigated by using the kinetic integral eigenmode equations derived from the ion gyrokinetic equation, the quasineutrality equation, the Ampère's law, and the massless electron approximation. Finite-beta effects on the toroidal force balance in the helical systems are taken into account by the stellarator expansion method. The ideal MHD ballooning mode equation is shown to be derived from the kinetic eigenmode equation in the fluid limit. Also, the Mercier criterion

obtained from the ideal MHD ballooning equation confirms that, in the helical systems, the negative magnetic shear combined with the Shafranov shift has a destabilizing effect by making both normal and geodesic curvatures unfavorable.

The kinetic integral eigenmode equations are numerically solved to obtain the real frequency, the growth rate, and the mode structure of the electromagnetic microinstability at the core region ($r/a \simeq 0.6$) in the LHD-like configuration with no net current. Their dependences on the plasma beta β, the poloidal wave number k_θ, and the magnetic shear parameter $\hat{s}$ are clarified. Stabilization of the ITG mode and destabilization of the KBM by increasing β are verified. The KBM at the high beta ($\beta \gtrsim 0.02$) has larger growth rates and wider unstable wave number regions than the ITG at the low beta ($\beta \lesssim 0.01$). Therefore, the KBM is expected to cause the anomalous transport in the high-beta case. In the low-beta case ($\beta < 0.03$), the KBM is stabilized by the strong (negative) magnetic shear while, in the high-beta case ($\beta > 0.03$), it is stabilized by the weak magnetic shear. These tendencies also correlate with the Mercier parameter, which contains effects of the field-line bending and the normal and geodesic curvatures. It is found under the present conditions that the KBM-unstable regions in β and $\hat{s}$ are narrower than the Mercier-unstable regions. Thus, kinetic effects such as the Landau damping and the finite gyroradii are considered to play a role of stabilization of the electromagnetic modes so that, for short wave lengths, their stability is better than predicted from the Mercier criterion based on the ideal MHD. This is consistent with the experimental result of the LHD plasma confinement in the Mercier-unstable region. However, the LHD experiment shows a better confinement for the inward magnetic axis shift with unfavorable magnetic curvature [7, 8], which cannot be explained by the present linear analysis. Also, effects of trapped particles, collisions, and more complete magnetic geometry are not considered here. These remain as future problems.

Acknowledgments

The authors thank Dr. N. Nakajima, Dr. K. Ichiguchi, Dr. M. Yokoyama, and Dr. Yamagishi for useful discussions on MHD equilibria and stability of helical plasmas. This work is supported in part by the Japanese Ministry of Education, Culture, Sports, Science, and Technology, Grant Nos. 12680497 and 14780387.

---

[1] W. Horton, Rev. Mod. Phys. **71**, 735 (1999).
[2] A. M. Dimits, G. Bateman, M. A. Beer, *et al.*, Phys. Plasmas **7**, 969 (2000).
[3] W. M. Tang, J. W. Connor, and R. J. Hastie, Nucl. Fusion **20**, 1439 (1980).
[4] T. Kuroda, H. Sugama, R. Kanno, and M. Okamoto, J. Phys. Soc. Jpn. **69**, 2485 (2000).
[5] G. Rewoldt, L.-P. Ku, W. M. Tang, H. Sugama, N. Nakajima, K. Y. Watanabe, S. Murakami, H. Yamada, and W. A. Cooper, Nucl. Fusion **42**, 1047 (2002).
[6] J. L. V. Lewandowski, Phys. Plasmas **10**, 4053 (2003).
[7] O. Motojima, N. Ohyabu, A. Komori, *et al.*, Nucl. Fusion **43**, 1674 (2003).
[8] H. Yamada, A. Komori, N. Ohyabu, *et al.*, Plasma Phys. Control. Fusion **43**, A55 (2001).
[9] O. Yamagishi, Y. Nakamura, K. Kondo, and N. Nakajima, Phys. Plasmas **10**, 2871 (2003).
[10] J. Q. Dong, L. Chen, and F. Zonca, Nucl. Fusion **39**, 1041 (1999).
[11] T. M. Antonsen, Jr. and B. Lane, Phys. Fluids **23**, 1205 (1980).
[12] P. J. Catto, W. M. Tang, and D. E. Baldwin, Plasma Phys. **23**, 639 (1981).
[13] H. Sugama, Phys. Plasmas **6**, 3527 (1999).
[14] N. Nakajima, Phys. Plasmas **3**, 4545 (1996).
[15] J. M. Green and J. L. Johnson, Phys. Fluids **4**, 875 (1961).
[16] J. P. Freidberg, *Ideal Magnetohydrodynamics* (Plenum Press, 1987), p. 218.
[17] B. Coppi, A. Ferreira, J. W.-K. Mark, and J. J. Ramos, Nucl. Fusion **19**, 715 (1979).

[18] R. D. Hazeltine and J. D. Meiss, *Plasma Confinement* (Addison-Wesley, Redwood City, California, 1992), p. 298.
[19] R. L. Dewar and A. H. Glasser, Phys. Fluids **26**, 3038 (1983).
[20] M. Wakatani, *Stellarator and Heliotron Devices* (Oxford University Press, 1998), p. 98.
[21] K. Ichiguchi, N. Nakajima, M. Okamoto, Y. Nakamura, and M. Wakatani, Nucl. Fusion **33**, 481 (1993).

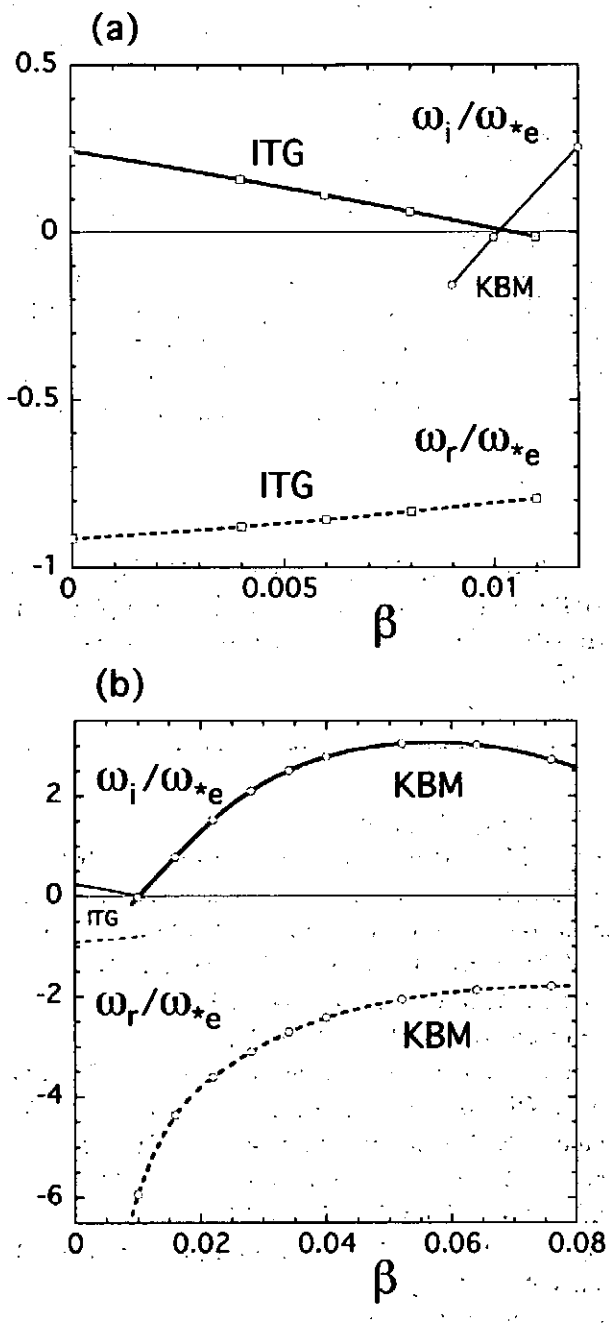

FIG. 1: Normalized growth rate ω_i/ω_{*e} and real frequency ω_r/ω_{*e} as a function of β for the ITG mode (a) and the KBM (b). Parameters used here are $L = 2$, $M = 10$, $q = 2$, $\hat{s} = -1$, $\theta_k = 0$, $\alpha_0 = 0$, $\eta_i = \eta_e = 3.5$, $\epsilon_n \equiv L_n/R_0 = 0.3$, $\tau_e \equiv T_e/T_i = 1$, $\epsilon_h/\epsilon_t = 1$, and $k_\theta \rho_{Ti} = 0.5$ (for the ITG mode), 0.35 (for the KBM).

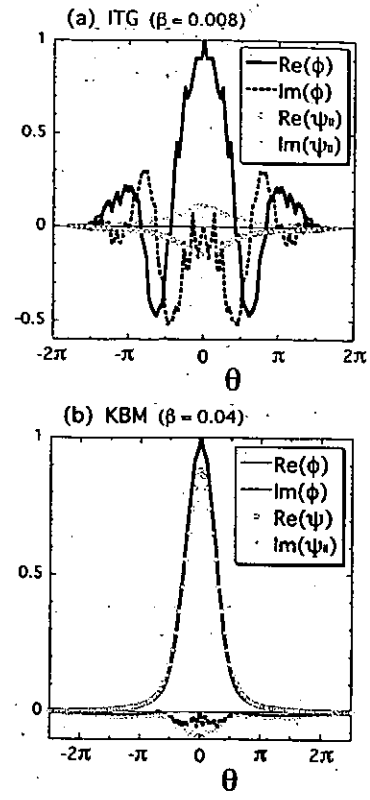

FIG. 2: Eigenfunctions $\phi(\theta)$ and $\psi_\parallel(\theta)$ of the ITG mode for $\beta = 0.008$ (a) and of the KBM for $\beta = 0.04$ (b). Other parameters used here are the same as in Fig. 1.

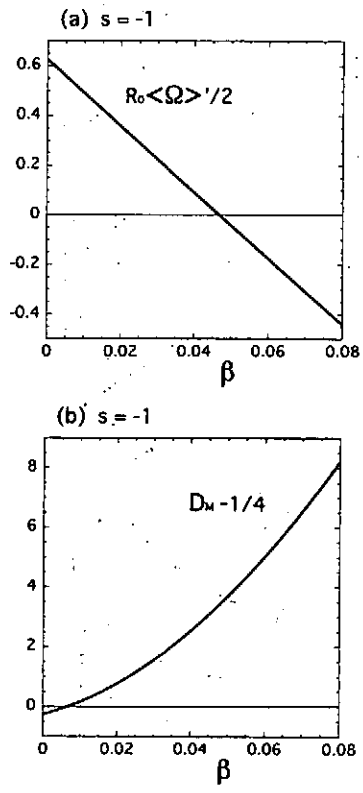

FIG. 3: Averaged normal curvature $R_0\langle\Omega\rangle'/2$ (a) and Mercier parameter $D_M - 1/4$ (b) as a function of β for the same parameters as in Fig. 1.

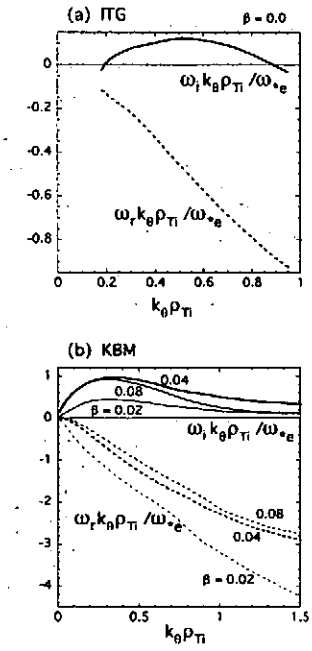

FIG. 4: Normalized growth rate $\omega_i k_\theta \rho_{Ti}/\omega_{*e}$ and real frequency $\omega_r k_\theta \rho_{Ti}/\omega_{*e}$ as a function of $k_\theta \rho_{Ti}$ for the ITG mode (a) and for the KBM (b). Here, $\beta = 0$ for the ITG mode and $\beta = 0.01$, 0.02, 0.04, 0.08 for the KBM are used. Other Parameters are the same as in Fig. 1.

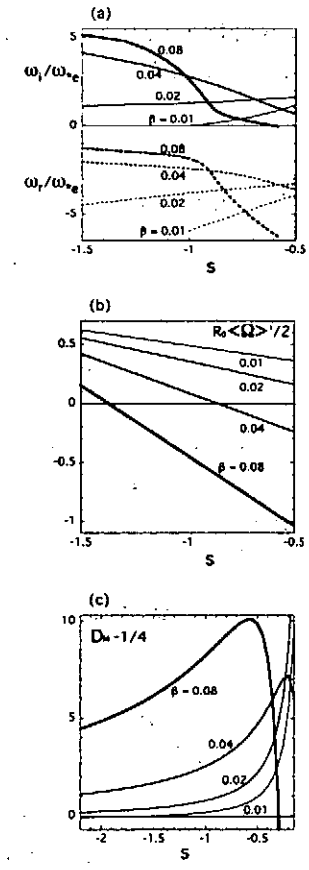

FIG. 5: Normalized real frequency ω_r/ω_{*e} and growth rate ω_i/ω_{*e} of the KBM for $k_\theta \rho_{Ti} = 0.35$ (a), averaged normal curvature $R_0\langle\Omega\rangle'/2$ (b), and Mercier parameter $D_M - 1/4$ (c) as a function of the magnetic shear parameter $\hat{s}$. Here, $\beta = 0.01$, 0.02, 0.04, and 0.08 are used. Other Parameters are the same as in Fig. 1.

Recent Issues of NIFS Series

NIFS-769 S.-I. Itoh, K. Itoh and S. Toda
Statistical Theory of L-H Transition and its Implication to Threshold Database
Jan. 2003

NIFS-770 K. Itoh
Summary: Theory of Magnetic Confinement
Jan. 2003

NIFS-771 S.-I. Itoh, K. Itoh and S. Toda
Statistical Theory of L-H Transition in Tokamaks
Jan. 2003

NIFS-772 M. Stepic, L. Hadzievski and M.M. Skoric
Modulation Instability in Two-dimensional Nonlinear Schrodinger Lattice Models with Dispersion and Long-range Interactions
Jan. 2003

NIFS-773 M.Yu. Isaev, K.Y. Watanabe, M. Yokoyama and K. Yamazaki
The Effect of Hexapole and Vertical Fields on α-particle Confinement in Heliotron Configurations
Mar. 2003

NIFS-774 K. Itoh, S.-I. Itoh, F. Spineanu, M.O. Vlad and M. Kawasaki
On Transition in Plasma Turbulence with Multiple Scale Lengths
May 2003

NIFS-775 M. Vlad, F. Spineanu, K. Itoh, S.-I. Itoh
Intermittent and Global Transitions in Plasma Turbulence
July 2003

NIFS-776 Y. Kondoh, M. Kondo, K. Shimoda, T. Takahashi and K. Osuga
Innovative Direct Energy Conversion Systems from Fusion Output Thermal Power to the Electrical One with the Use of Electronic Adiabatic Processes of Electron Fluid in Solid Conductors.
July 2003

NIFS-777 S.-I. Itoh, K. Itoh and M. Yagi
A Novel Turbulence Trigger for Neoclassical Tearing Modes in Tokamaks
July 2003

NIFS-778 T. Utsumi, J. Koga, T. Yabe, Y. Ogata, E. Matsunaga, T. Aoki and M. Sekine
Basis Set Approach in the Constrained Interpolation Profile Method
July 2003

NIFS-779 Oleg I. Tolstikhin and C. Namba
CTBC A Program to Solve the Collinear Three-Body Coulomb Problem: Bound States and Scattering Below the Three-Body Disintegration Threshold
Aug. 2003

NIFS-780 Contributions to 30th European Physical Society Conference on Controlled Fusion and Plasma Physics (St.Petersburg, Russia, 7-11 July 2003) from NIFS
Aug. 2003

NIFS-781 Ya. I. Kolesnichenko, K. Yamazaki, S. Yamamoto, V.V. Lutsenko, N. Nakajima, Y. Narushima, K. Toi, Yu. V. Yakovenko
Interplay of Energetic Ions and Alfvén Modes in Helical Plasmas
Aug. 2003

NIFS-782 S.-I. Itoh, K. Itoh and M. Yagi
Turbulence Trigger for Neoclassical Tearing Modes in Tokamaks
Sep. 2003

NIFS-783 F. Spineanu, M. Vlad, K. Itoh, H. Sanuki and S.-I. Itoh
Pole Dynamics for the Flierl-Petviashvili Equation and Zonal Flow
Sep. 2003

NIFS-784 R. Smirnov, Y. Tomita, T. Takizuka, A. Takayama, Yu. Chutov
Particle Simulation Study of Dust Particle Dynamics in Sheaths
Oct. 2003

NIFS-785 T.-H. Watanabe and H. Sugama
Kinetic Simulation of Steady States of Ion Temperature Gradient Driven Turbulence with Weak Collisionality
Nov. 2003

NIFS-786 K. Itoh, K. Hallatschek, S. Toda, H. Sanuki and S.-I. Itoh
Coherent Structure of Zonal Flow and Nonlinear Saturation
Dec. 2003

NIFS-787 S.I. Itoh, K. Itoh, M. Yagi and S. Toda
Statistical Theory for Transition and Long-time Sustainment of Improved Confinement State
Dec. 2003

NIFS-788 A. Yoshizawa, S.-I. Itoh, K. Itoh and N. Yokoi
Dynamos and MHD Theory of Turbulence Suppression
Dec. 2003

NIFS-789 V.D. Pustovitov
Pressure-induced Shift of the Plasma in a Helical System with Ideally Conducting Wall
Jan. 2004

NIFS-790 S. Koikari
Rooted Tree Analysis of Runge-Kutta Methods with Exact Treatment of Linear Terms
Jan. 2004

NIFS-791 T. Takahashi, K. Inoue, N. Iwasawa, T. Ishizuka and Y. Kondoh
Losses of Neutral Beam Injected Fast Ions Due to Adiabaticity Breaking Processes in a Field-Reversed Configuration
Feb. 2004

NIFS-792 T.-H. Watanabe and H. Sugama
Vlasov and Drift Kinetic Simulation Methods Based on the Symplectic Integrator
Feb. 2004

NIFS-793 H. Sugama and T.-H. Watanabe
Electromagnetic Microinstabilities in Helical Systems
Feb. 2004